EXPERIMENTAL EVALUATION OF THE MIMO WIDEBAND CHANNEL TEMPORAL VARIATION

J. W. Wallace[(1)], B. T. Maharaj[(2)], M. A. Jensen[(1)]

[(1)]Department of Electrical and Computer Engineering, Brigham Young University, 459 CB, Provo, UT 84602, USA, Email: wall@ieee.org, jensen@ee.byu.edu

[(2)]Department of Electrical, Electronic and Computer Engineering, University of Pretoria, Lynnwood Road 0002, Pretoria, South Africa, Email: sunil.maharaj@up.ac.za

I. INTRODUCTION

With perfect channel state information (CSI) at the receiver and/or transmitter, multiple-input multiple-output (MIMO) wireless systems exhibit a large capacity improvement over their single-input single-output (SISO) counterparts. However, when the MIMO channel is time variant, CSI is either imperfect or unavailable, leading to severe reductions in the available capacity [1]. Although a few studies have appeared that characterize the extent of time variation in measured MIMO channels [2], [3], to our knowledge there is no work that presents a comprehensive framework for characterizing and modeling this phenomenon.

In this paper, we present a framework for characterizing MIMO channel time variation based on wideband 8×8 MIMO channel measurements in indoor environments. The paper introduces several new metrics which are useful for assessing the severity of time variation. Furthermore, this work investigates the ability of two different time-varying models to capture key behaviors observed in the measured MIMO channels.

II. MEASUREMENTS

Fig. 1 shows a block diagram of the wideband 8×8 MIMO channel sounder developed at Brigham Young University (BYU). At the transmitter, an arbitrary waveform generator creates a multi-tone signal with up to 100 MHz of instantaneous bandwidth, which is up-converted to a range between 2-8 GHz, amplified, and fed through an 8-way switch to the transmit array. At the receive side, an 8-way switch routes signals from the array to a common RF receiver consisting of low noise amplification, down-conversion, automatic gain control (AGC), and up to 500-MS/s PC-based A/D conversion and storage. Control of the antenna switches is accomplished by a synchronization unit that scans all possible antenna combinations with a selectable dwell time. The transmit and receive antennas are 8-element uniform circular arrays consisting of omnidirectional monopole elements with $\lambda/2$ inter-element spacing. Highly stable 10 MHz rubidium time/frequency references provide system synchronization at transmit and receive.

The number of consecutive channel snapshots that can be acquired is limited by the memory depth (512 MB) and sample rate (12.5-500 MS/s) of the A/D card. A "multiple record" feature allows delays to be placed between channel snapshots, thus extending the acquisition length. The number of locations probed in a single campaign is limited by hard drive space on the PC, where 100 GB can hold about 200 locations.

MIMO channel time variation was studied by placing the transmitter in a fixed position and moving the receiver at a constant speed over a prescribed path of up to 4.5 m. The transmit signal consisted of 80 tones with 1 MHz separation, an antenna dwell time of 50 μS, and a center frequency of either 2.55 or 5.2 GHz. Channels were acquired either back-to-back every 3.2 ms (fast mode) or with multiple record every 25.6 ms (slow mode), allowing investigation of both small- and large-scale variations.

For the indoor data presented here, the transmitter was stationary in a hallway, while the receiver was placed in 8 different rooms. In each room, different measurements were performed. First, measurements with the transmitter turned off and the receiver stationary indicated that neglibible interference was present in the 2.55 GHz band. Second, a measurement with the transmitter and receiver stationary showed that the Doppler component due to the channel was less than 1 Hz, much smaller than the 10-20 Hz Doppler component observed when the receiver was moving at 0.3 m/s. Finally, measurements with the receiver moving (0.3 m/s) with fast and slow acquisition revealed that the slow sample rate was sufficient to capture the channel time variation.

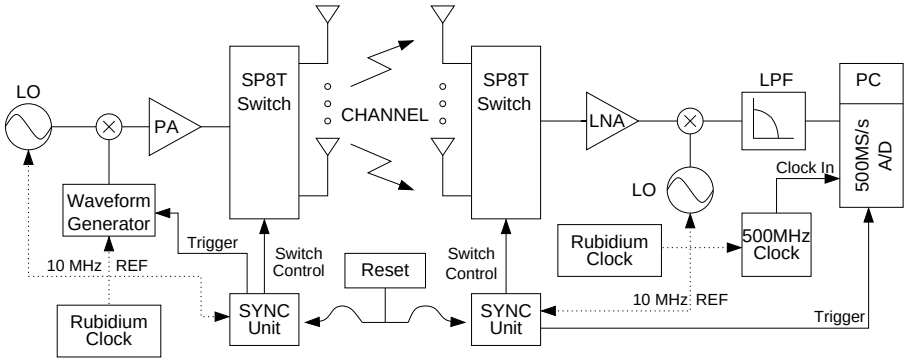

Fig. 1. Simplified block diagram of the 8×8 wideband MIMO channel sounder used to measure time variation of indoor and outdoor MIMO channels

III. MIMO TIME-VARIATION METRICS

Key to this work are a set of metrics that indicate the degree of time variability of measured channels. Our goal in defining these metrics is not only to allow various measured channels to be classified, but also to assess the accuracy of time-varying models and to provide a connection between MIMO channel variation and the performance of other communications layers. Although our metrics are intended for *time*-varying channels, we characterize variation versus distance, allowing the results to be scaled for different movement speeds.

A. Eigenvalue/Eigenvector Metrics

The singular value decomposition (SVD) of a single channel matrix $\mathbf{H}$ is given by $\mathbf{H} = \mathbf{USV}^H$, where $\mathbf{U}$ and $\mathbf{V}$ are the matrices of left and right singular vectors, and $\mathbf{S}$ is the diagonal matrix of ordered singular values. We refer to $\sigma_i(\mathbf{H}) = S_{ii}^2$ as the ith channel eigenvalue and column vectors $\mathbf{u}_i$ and $\mathbf{v}_i$ as the ith transmit and receive eigenvectors, respectively. Since σ_i represents a power gain, we can apply standard single-antenna metrics to each eigenvalue. Eigenvalue level crossing rate for the the ith eigenvalue (ELCR_i) is computed as the number of times that $\sigma_i(\mathbf{H})$ drops below a specified threshold divided by the distance traveled. Eigenvalue average fade duration (EAFD_i) is the average fraction of path distance that the waveform lies below the threshold. The threshold will depend on the application, and in this work we use 2 dB below the mean.

Similarly, eigenvector angular deviation (EAD) quantifies how quickly the transmit and receive eigenvectors rotate in complex M-dimensional space, where M is the number of antenna elements. We define EAD as

$$\theta_k = \frac{1}{N-k}\sum_{n=1}^{N-k}\cos^{-1}|\mathbf{v}^{(n)H}\mathbf{v}^{(n+k)}|, \tag{1}$$

where k is the distance between two channel snapshots, N is the total number of snapshots, and $\mathbf{v}^{(n)}$ is the nth snapshot of a given left or right singular vector.

B. Capacity Degradation

Although the eigenchannel metrics are useful for system specification and design, they do not indicate the loss of channel quality in an information theoretic sense. Consider the case of *transmit CSI degradation* (TCD) where the receiver has perfect CSI but the transmitter only has the delayed channel estimate $\hat{\mathbf{H}}$. We may define capacity for delayed transmit CSI as

$$C_T = \log_2\left|\frac{\mathbf{HQ}(\hat{\mathbf{H}})\mathbf{H}^H}{\sigma^2}+\mathbf{I}\right|, \tag{2}$$

where $\mathbf{H}$ is the true channel, σ^2 is the receiver noise variance, $\mathbf{Q}(\hat{\mathbf{H}})$ is the optimal transmit covariance given by the water-filling solution (assuming $\mathbf{H}=\hat{\mathbf{H}}$), $\mathbf{I}$ is the identity matrix, $\mathrm{Tr}\{\mathbf{Q}\}\le P_T$, and P_T is total transmit power. In the results that follow, P_T and σ^2 are chosen such that the average SISO SNR is 10 dB. As the estimate $\hat{\mathbf{H}}$ becomes increasingly outdated, C_T will tend to decrease. The term $d_T$represents the distance at which the delayed capacity drops below the uninformed transmit capacity (C_T with $\mathbf{Q}=\mathbf{I}$).

Next, consider the case of *receive CSI degradation* (RCD), where both transmit and receive have outdated CSI. With perfect CSI, parallel channels may be formed by using the channel matrix singular vectors as beamformers. Imperfect

estimates of the channel $\hat{\mathbf{H}} = \hat{\mathbf{U}}\hat{\mathbf{S}}\hat{\mathbf{V}}^H$ cause "cross-talk" among these parallel channels. Since we make no assumptions about the distribution of $\mathbf{H}$, we consider the worst case where the interference is i.i.d. Gaussian, resulting in

$$C_R = \sum_i \log_2(1 + p_i S_{ii}/q_i), \tag{3}$$

where $q_i = \left\{\mathbf{MPM}^H\right\}_{ii} + \sigma^2$, $\mathbf{M} = \hat{\mathbf{U}}^H\mathbf{H}\hat{\mathbf{V}} - \mathbf{\Phi}\hat{\mathbf{S}}$, $\mathbf{P} = \mathrm{diag}(\mathbf{p})$, and $\mathbf{\Phi}$ is a complex diagonal matrix whose diagonal elements have unit magnitude. In this work, we assume $\arg(\Phi_{ii}) = \arg(\{\hat{\mathbf{U}}^H\mathbf{H}\hat{\mathbf{V}}\}_{ii})$, thus masking the effect of average phase variations of the individual eigenchannels and focusing on the changing spatial structure. We refer to the point at which C_R drops to 50% of its maximum value as the distance d_R.

IV. TIME-VARIANT MIMO CHANNEL MODELS

Since accurate models are critical for the design and analysis of MIMO architectures, we investigate two different modeling strategies for time-variant MIMO channels: (1) a random matrix model following the multivariate complex normal (MVCN) distribution and (2) a time-variant clustering (TVC) model.

A. MVCN Model

We represent the complex gain from the jth transmitter to the ith receiver at time index n for a single frequency bin as $H_{ij}^{(n)}$. If these gains follow a (possibly time-varying) MVCN distribution in both time and space, the spatio-temporal variation of the MIMO channel is completely characterized by the multivariate mean ($\mathbf{M}$) and covariance ($\mathbf{R}$) of $\mathbf{H}$. Here, we consider a process characterized by a mean and covariance that vary slowly in time, allowing estimation by weighted sample averages. In this work, we apply an exponential window, of the form $w_s = \exp(-|s/\ell_c|)$, where ℓ_c is the correlation length. If the process is determined to be nearly stationary over N_s samples, faithful estimates can be obtained with $4\ell_c = Ns$.

To determine a suitable value for ℓ_c, three different tests for multivariate normality were applied to the data: (1) Mardia's tests for multivariate skewness and (2) kurtosis [4], and (3) the Henze-Zirkler test [5]. Fig. 2 depicts the average rejection rates for a significance level of 5% and a varying record length (sample size) for 2×2 subsets of the MIMO indoor data at 2.55 GHz. Very similar plots are obtained for 5.2 GHz. The results indicate that over distances of $4-8\lambda$ the rejection rates are acceptable, and we therefore let $\ell_c = 2\lambda$.

Once the time-varying mean and covariance have been estimated from the data, we assume that the covariance is separable in the time and space dimensions or $R_{ij,k\ell}^{(n,m)} = R_{S,ij,k\ell}^{(n)} R_T^{(n,m)}$. Synthetic channels can then be generated stepwise as

$$B_{ij}^{(n)} = \sum_{n'} X_{T,nn'} A_{ij}^{(n')} \qquad\qquad H_{ij}^{(n)} = \sum_{i'j'} X_{S,ij,i'j'}^{(n)} A_{i'j'}^{(n)}, \tag{4}$$

where $\mathbf{X}_T = \mathbf{R}_T'^{1/2}$, $\mathbf{X}_S = \mathbf{R}_S^{(n)1/2}$, $R'_{T,nn'} = R_T^{(n,n'-n)}$, i and j are stacked when used as a covariance index, and $A_{ij}^{(n')}$ are matrices of i.i.d. complex normal elements.

B. TVC Model

Another modeling approach for the time-varying MIMO channel is an extension of the cluster modeling strategy described in [6]. In this strategy, we first obtain the double-directional Bartlett spatial spectrum of the measured response for time step n. We then assume that the true diffuse arrival power spectrum can be represented as a weighted set of basis functions, and estimate the time-variant weight coefficients for this representation based on the observed Bartlett spectrum. Synthetic channels may then be realized by randomly generating L rays for each of the basis functions such that they obey the estimated diffuse arrival power spectrum. Given the space limitations of this paper, the details of this modeling strategy will be provided in a future publication.

C. Model Comparisons

We now apply the proposed time-variation metrics directly to measured data as well as synthetic channels generated with the MVCN and TVC models. When computing covariance, mean, and time-variation metrics from data, we consider 8 frequency bins separated by 10 MHz as statistically independent realizations, thus creating an effectively larger sample size. For the models at each location, 10 independent temporal evolutions (realizations) are considered.

Fig. 3 shows a typical result for the RCD capacity metric (3), taken from an indoor location at 5.2 GHz. In most cases, the RCD capacity for the MVCN model dropped too quickly and the TVC model provided a better fit. On the other hand, the MVCN model matched TCD capacity very well. Tables I and II list the metrics applied to measured data

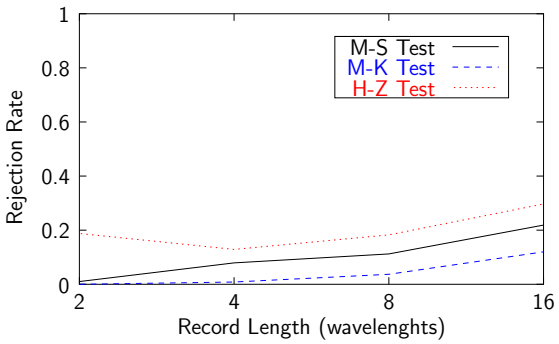

Fig. 2. Average rejection rates for three multivariate normal tests for all indoor locations at 2.55 GHz.

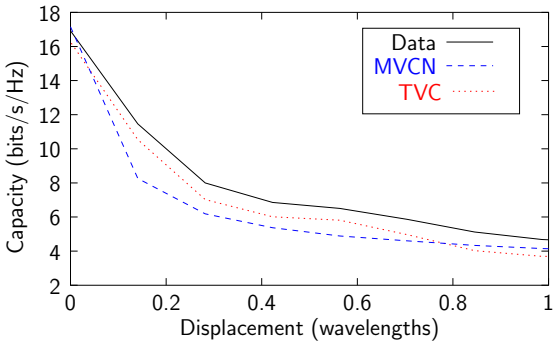

Fig. 3. Typical RCD capacity plot taken from an indoor location at 5.2 GHz.

TABLE I
METRICS FOR 2.55 GHZ INDOOR DATA/MODELS

	d_R			d_T		
Loc.	Data	MVCN	TVC	Data	MVCN	TVC
1	0.28	0.14	0.21	7.8	6.3	≥ 10
2	0.28	0.14	0.28	≥ 10	4.4	≥ 10
3	0.21	0.14	0.14	1.7	0.3	≥ 10
4	0.21	0.14	0.21	3.3	2.6	≥ 10
5	0.21	0.14	0.21	7.2	5.5	≥ 10
6	0.21	0.14	0.21	≥ 10	≥ 10	≥ 10
7	0.21	0.14	0.21	2.0	0.4	≥ 10
8	0.21	0.14	0.21	3.0	0.8	≥ 10
	ELCR_1			ELCR_2		
Loc.	Data	MVCN	TVC	Data	MVCN	TVC
1	0.31	0.73	0.39	0.40	0.97	0.44
2	1.21	1.42	0.37	1.05	1.55	0.41
3	0.81	1.12	0.60	0.52	0.99	0.61
4	0.58	0.72	0.28	0.67	1.01	0.48
5	0.76	0.98	0.46	0.47	1.11	0.53
6	0.40	0.70	0.37	0.56	0.99	0.46
7	0.33	0.71	0.32	0.44	0.81	0.35
8	0.72	0.94	0.44	0.56	1.04	0.61

TABLE II
METRICS FOR 5.2 GHZ INDOOR DATA/MODELS

	d_R			d_T		
Loc.	Data	MVCN	TVC	Data	MVCN	TVC
1	0.28	0.28	0.28	≥ 10	≥ 10	≥ 10
2	0.28	0.28	0.28	≥ 10	≥ 10	≥ 10
3	0.28	0.14	0.14	3.38	1.8	≥ 10
4	0.28	0.14	0.28	≥ 10	≥ 10	≥ 10
5	0.28	0.14	0.28	≥ 10	≥ 10	≥ 10
6	0.28	0.14	0.28	≥ 10	≥ 10	≥ 10
7	0.28	0.28	0.28	≥ 10	≥ 10	≥ 10
8	0.28	0.14	0.14	≥ 10	≥ 10	≥ 10
	ELCR_1			ELCR_2		
Loc.	Data	MVCN	TVC	Data	MVCN	TVC
1	0.25	0.61	0.23	0.35	0.67	0.28
2	0.25	0.57	0.37	0.42	0.66	0.53
3	0.22	0.65	0.58	0.57	0.80	0.57
4	0.41	0.64	0.33	0.56	0.66	0.41
5	0.25	0.60	0.25	0.41	0.67	0.51
6	0.42	0.72	0.30	0.47	0.80	0.35
7	0.20	0.69	0.31	0.31	0.52	0.38
8	0.43	0.63	0.42	0.51	0.79	0.47

and synthetic channels at 2.55 GHz and 5.2 GHz, respectively, where all metrics have units of wavelengths. Although the TVC model better predicts metrics associated with short-term variations (C_R, d_R, ELCR, and EAFD), the MVCN model more faithfully captures the long-term behavior (C_T and d_T).

V. CONCLUSION

Although MIMO systems exhibit high capacity with perfect CSI, imperfect CSI can lead to reductions in available capacity. This paper provided a number of new metrics for characterizing the time-variation of MIMO channels, useful for classifying channels, assessing modeling accuracy, and connecting time variation to the performance of higher communications layers. A random matrix model based on the MVCN distribution and a cluster model both showed promise in capturing the key behaviors of the time-varying channels.

REFERENCES

[1] A. Goldsmith, S. A. Jafar, N. Jindal, and S. Vishwanath, "Capacity limits of MIMO channels," *IEEE Trans. Inf. Theory*, vol. 21, pp. 684–702, Jun. 2003.
[2] D. P. McNamara, M. A. Beach, and P. N. Fletcher, "Experimental investigation of the temporal variation of MIMO channels," in *Proc. 2001 IEEE 54th Veh. Technol. Conf.*, Atlantic City, NJ, Oct. 7-11 2001, pp. 1063–1067.
[3] H. Xu, M. Gans, D. Chizhik, J. Ling, P. Wolniansky, and R. Valenzuela, "Spatial and temporal variations of MIMO channels and impacts on capacity," in *Proc. 2002 IEEE Intl. Conf. Commun.*, vol. 1, New York, NY, Apr. 28-May 2 2002, pp. 262–266.
[4] K. V. Mardia, J. T. Kent, and J. M. Bibby, *Multivariate analysis*. Academic Press, 1979.
[5] N. Henze and B. Zirkler, "A class of invariant consistent tests for multivariate normality," *Commun. Statist.-Theor. Meth.*, vol. 19, no. 10, pp. 3595–3618, 1990.
[6] J. Wallace, H. Özcelik, M. Herdin, E. Bonek, and M. Jensen, "A diffuse multipath spectrum estimation technique for directional channel modeling," in *Proc. 2004 IEEE Intl. Conf. Commun.*, vol. 6, Paris, France, Jun. 20-24 2004, pp. 3183–3187.